ARTICLE OPEN

Check for updates

# *In-operando* analysis of the corrosion patterns and rates under magnetic fields using metallic film

Cirlei Igreja Nascimento Mitre[1], Giancarlo Tosin[2] and Luiz Alberto Colnago[3]✉

Magnets, or electromagnets, are common components in everyday appliances and are widely used in medicine, industries, transportation, and electrical power systems. It is known that the magnetic field (**B**) can mitigate or aggravate metallic corrosion; however, this apparent contradictory effect is still not fully understood. In this study, we demonstrate a simple method to monitor *in-operando* the effect of permanent magnets (**B**) on corrosion processes using metallic film (copper clad laminate), $FeCl_3$ solution as corrosive medium, and digital camera to record the experiments. The results show that homogeneous and inhomogeneous **B** decrease or increase the corrosion rate, respectively. The homogeneous and inhomogeneous **B** also shows different corrosion patterns and induces rotation of the corrosive medium indicating the presence of the Lorentz force. The procedure proposed can also be applied to other metals and corrosive media providing valuable information on the corrosion process in the presence of **B** in several environmental conditions.

*npj Materials Degradation* (2022)6:24 ; https://doi.org/10.1038/s41529-022-00233-5

## INTRODUCTION

Metallic corrosion is a major problem in modern society, as it affects all metallic materials from small electronic components to major infrastructures[1,2]. Corrosion often results in costly and sometimes catastrophic incidents with safety and environmental consequences. It is estimated that the direct and indirect costs of corrosion amount to US$ 2.5 trillion globally, which is equivalent to 3.4% of the world's gross product[3].

It is known that magnetic field (**B**) can mitigate or aggravate metallic corrosion; nevertheless, the phenomenon is not fully understood[4–12]. Therefore, it is paramount to understand the apparent contradictory effect of **B** of permanent magnets, or electromagnets on the corrosion rate and pattern of metallic components to avoid premature failure of electrical motors, generators, transformers, sensors, actuators, which are widely used in everyday life appliances, as well as in medicine, industries, transportation, and electrical power systems.

Many authors have studied the effects of magnetic field on the corrosion rate and observed that magnetic field decreases[4–8], increases[5–12], or even has no effect[9] on it. This ambiguous effect of the magnetic field observed on corrosion processes is attributed to differences in the corrosive medium[5,9], metal type[4], magnetic field strength[6,12], direction in relation to the metal surface[5,6], or the presence of gradients[7]. In these experiments, the magnetic field effect was detected by changes in the corrosion rate obtained by mass loss[5,8,11] and change of the corrosion potential or corrosion current density at polarization curves[6–8]. The effect of magnetic field on the surface of corroded metals has been analyzed using scanning electron microscopy (SEM)[5,9] or optical images[8].

Only a few studies have been published without applied electrical potential[4,9]. Sagawa[4] studied the corrosion of copper and iron sheet in nitric acid solution under a magnetic field applied perpendicular to the surfaces. He observed that the magnetic field reduces the corrosion rate and the corrosion products formed during the reaction appear to be attracted by the magnet pole. He explains the mitigating effect of the **B** by the absence of vortexes caused by Lorentz force in the solution and that **B** represses the diffusion of the corrosion products in the metal surface and this increases the diffusion layer that consequently reduces the rate of mass-transport-controlled reaction.

Ang et al.[9] studied the effect of **B** parallel to the metallic surface. They observed an increase in the copper corrosion rate in HCl and NaOH solutions but there was no effect when the corrosive agent was NaCl solution. They explained these observations indicating that the mass transfer is the primary mode for the corrosions in HCl and NaOH solutions and the reaction rate is increased by the magnetohydrodynamics effect caused by **B**. On the other hand, for NaCl, the main mode is the electron charge transfer and no effect of the **B** was expected in the reaction rate.

In this study, we introduce a simple and fast way to visually monitor the positive or negative effect of **B** on metallic corrosion processes *in operando* using a digital camera and metallic thin film (copper clad laminate discs—CCL). Corrosion of CCL discs in the absence or presence of homogeneous or inhomogeneous **B** shows several etching patterns and different reaction rates, which are not easily observed using metal bulks. In addition, a rotation of the corrosive medium occurs when the corrosion reaction is performed in the presence of **B**, indicating the effect of the Lorentz force. This simple, fast, and real-time procedure demonstrated here with CCL and digital cameras could also be applied to other metals and other corrosive environments.

## RESULTS AND DISCUSSIONS

We used CCL discs as metallic thin film and $FeCl_3$ solution as a corrosive medium to prove the concept. CCL and $FeCl_3$ were chosen because they are easily found commercial products used to make printed circuit boards. In this corrosion process, metallic

[1]Instituto de Química de São Carlos, Universidade de São Paulo, Avenida Trabalhador São Carlense 400, 13566-590 São Carlos, São Paulo, Brazil. [2]LMA Magnet Consultancy, Rua Filomeno Rispoli 509, 13564-200 São Carlos, São Paulo, Brazil. [3]Embrapa Instrumentação, Rua 15 de Novembro, 1452 - Centro, 13570-970 São Carlos, SP, Brazil. ✉email: luiz.colnago@embrapa.br

Cu is initially oxidized by $FeCl_3$ to form CuCl that is subsequently oxidized by another $FeCl_3$ to form $CuCl_2$, which is a water-soluble product that facilitates metallic dissolution[13,14]. The corrosion progress on the copper film is visually observed by color contrast between the regions with and without metallic materials (Figs. 1–5). Thus, the static and dynamic corrosion processes can be recorded *in operando*, using digital or cellphone cameras, that is, without requiring the use of sophisticated equipment.

### Corrosion of CCL disc in the absence of magnetic field

We first studied the corrosion of the CCL disc in the absence of **B** as a control experiment to compare with the experiments performed in the presence of homogeneous and inhomogeneous **B**. We also implemented the experiments blocking and not blocking the edge of CCL discs with the cell wall as different corrosion rates and patterns were observed in these conditions.

In the first experiments, using the large cells in absence of **B**, we observed that the corrosion pattern was not constant. The corrosion always starts from the disc edges but, sometimes it occurred symmetrically, as in Fig. 1a or asymmetrically, as in Fig. 1b. After performing some experiments, we determined that the symmetrical pattern occurs when the cells were leveled and the asymmetrical ones when the cells were off-level in the order of 1 degree. We also observed that the most corroded area is observed in the elevated region which may suggest that the reaction is more effective with less solution layer and faster absorption of oxygen from the air to oxidized $FeCl_2$ to $FeCl_3$, ensuring the etching process. Therefore, the use of thin film shows the sensitiveness of corrosion to leveling and to the best of our knowledge, this is the first observation of this leveling effect. For this reason, the cells in all corrosion experiments shown in Figs. 2–5 were leveled.

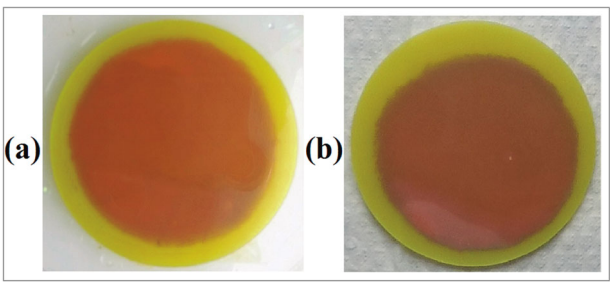


**Fig. 1 Leveling effect. a** Picture of the corroded CCL disc when the cell was leveled. **b** Picture of the corroded CCL disc when the cell was off level by ~1 degree.

Figure 2a shows pictures of CCL disc etched in $FeCl_3$ solution at 30, 60, 90, and 120 min using the big cell (BC) with 83.5 mm in diameter, which does not block the disc edge. The picture of the CCL disc at 30 min is identical to the disc picture at the beginning of the process. Some corrosion occurs at this time but it is not observed on the disc. Pictures at 60 and 90 min show a symmetrical etching of the copper film at its perimeter indicating that corrosion in this experimental setup occurs preferentially in this area. Corrosion occurs preferentially at the disc edge because copper in this area is etched by the ferric ions in the solution above it as well as by the ions from the extra solution beyond the CCL border. This process at the disc edge is known as the edge-effect[15,16]. The symmetrical corrosion pattern, from the disc edge to the center, was observed at 120 min and up to the end of the etching process at ~140 min.

Initially, we implemented the experiments with a small cell (SC), that blocks the 51 mm disc edge, using a taller small cell (TSC) with 51.2 mm of internal diameter that holds 30 ml of corrosive medium. However, it was not possible to monitor the reaction *in operando*, because the disc at the bottom of the cell was not visible, due to the low transparency of the corrosive medium (Supplementary Fig. 1a). Therefore, experiments with SC were performed with 10 ml of a corrosive medium to have the same solution thickness of BC. The corrosive medium was replaced by a new solution when it changed from light yellow to a green-brown opaque color. Corrosion experiments with three 10 ml of solution showed a similar corrosion pattern (Fig. 2b) when compared to experiments conducted with TSC (Supplementary Fig. 1b).

Figure 2b shows pictures of the CCL disc etched in $FeCl_3$ solution at 30, 120, 180, and 200 min in SC. Similarly, the corrosion process using the BC (Fig. 2a) the pictures did not show any visible etching up to 30 min. The etching in SC is only observed at ~100 min or longer, as presented in the pictures of 120, 180, and 200 min. These results indicate that the physical barrier (cell wall) on the edge of the CCL disc blocks the access to extra ferric ions. However, in SC, the etching process also started in a certain area of the disc edge (Fig. 2b, 120 min), due to some defect (gap) between the disc and the SC wall that allows access to extra ferric ions in comparison with other areas of the disc. To confirm this hypothesis, the corrosion experiment was also implemented using a disc with a small-sanded area (~0.3 mm) in the disc perimeter. Supplementary Fig. 2 confirms this hypothesis as the corrosion always started in the sanded area that allow preferential corrosion. After the beginning of the etching process in the defect region, all

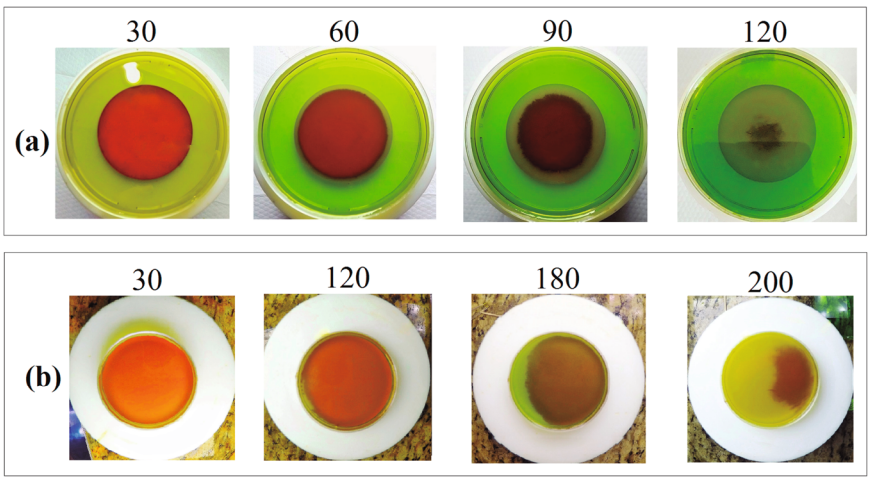


**Fig. 2 Corrosion of CCL disc in the absence of magnetic field. a** Pictures of the typical corrosion process that happens on CCL disc in $FeCl_3$ solution at 30, 60, 90, and 120 min in a big cell (BC). **b** Pictures of CCL disc in $FeCl_3$ solution at 30, 120, 180, and 200 min in small cell (SC).

metallic material is consumed from this point to the other areas of the disc, with no new etching point at the edge, resulting in an asymmetrical etching pattern (Fig. 2b, 180 and 200 min).

The edge or cut-edge effect is better seen when the corrosion is performed on a CCL with a 16-mm hole in the center of the disc (Fig. 3a) which clearly shows that the corrosion started from both edges (center and outside), but it is more pronounced on external border due to access to more $Fe^{3+}$ ions. Figure 3b shows that corrosion of the CCL disc with the ink-protected edge started at the region just after the ink, indicating that corrosion was not caused by the cut-edge effect, but by the edge effect.

Figures 1–3 demonstrated that the thin CCL film is a simple and rapid way to monitor metallic corrosion, *in operando*, when compared to other methods used to monitor corrosion processes like microscopy, profilometry, and interferometry[17–20]. Besides, the CCL film easily allows the observation of the reaction in real-time and the effects of leveling and obstruction edge.

### Corrosion of CCL disc in the presence of magnetic field

We used four experimental setups to study the macroscopic effects of magnetic field (**B**) on CCL corrosion (Fig. 8). The CCL disc in SC and BC on top of the big magnet, BMBC and BMSC setups, respectively (Fig. 8a-I and a-II) and on top of the small magnet, SMBC, and SMSC, respectively (Fig. 8b-III and b-IV).

### Corrosion using magnet bigger than CCL disc

Figure 4 shows the pictures of CCL discs etched in $FeCl_3$ solution in BMBC and BMSC setups. In these setups, the CCL discs rest in the most homogeneous region of the magnet (Fig. 8a) called here homogeneous **B**. Supplementary Video 1 illustrates the effect of **B** on the mass transport process that occurs at corrosive medium, in the BMBC setup (Fig. 8a-I).

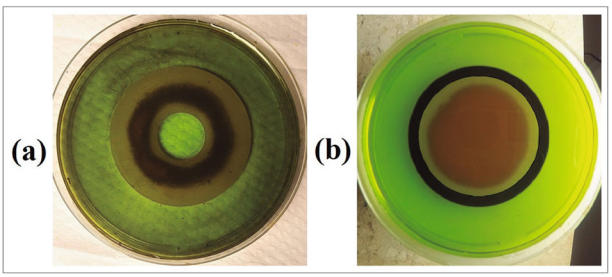


**Fig. 3 The edge effect. a** Picture of the CCL disc with a 16-mm hole in the center after the corrosion experiment. **b** Picture of the CCL disc corrosion with the ink-protected perimeter.

Figure 4a shows pictures of a typical corrosion process on the CCL disc at 30, 100, 160, and 300 min, using the BMBC setup (Fig. 8a-I). The picture of the CCL disc at 30 min (Fig. 4a) is identical to the disc picture at the beginning of the reaction. However, the corrosive solution in the presence of **B** rotates just after the contact between the solution and metal (Supplementary Video 1) indicating the corrosion reaction. This magnetohydrodynamic (MHD) phenomenon is frequently observed when electrochemical reactions, like corrosion, are performed in the presence of **B**[5,21–28]. However, the MHD phenomenon without the application of an electric field is rarely reported. Blaha[29] in 1950 and Davenport et al. in 2003[8] reported a similar rotation of the corrosive medium when the reaction was performed in presence of **B**. Davenport et al. attribute this rotation to the action of Lorentz force. Supplementary Video 1 demonstrates the counterclockwise rotation of the corrosive solution on the **B** south pole in the BMBC experiment and it is also observed in the BMSC setup. The solution rotates clockwise when the corrosion reaction is performed using **B** north pole suggesting the action of Lorentz force.

The picture of the CCL disc at 100 min (Fig. 4a) shows a symmetrical etching of the CCL disc edge similar to corrosion in the absence of **B** (Fig. 2a). However, the CCL etched area at 160 min in the presence of **B** (Fig. 4a) was much smaller than in the CCL disc at 120 min in absence of **B** (Fig. 2a), indicating a reduction of the corrosion rate. The protective effect of **B** is even more evident when comparing the corroded area of Fig. 2a and Fig. 4a. The equivalent corroded area observed at 120 min in absence of **B** (Fig. 2a) is only observed at 300 min in presence of **B** (Fig. 4a), indicating a reduction in the corrosion rate by more than a half.

Figure 4b shows pictures of the CCL disc in $FeCl_3$ solution at 30, 100, 160, and 300 min, using the BMSC setup (Fig. 8a-II). The corrosion pattern is similar to that observed in the beginning of the process using SC in the absence of **B** (Fig. 2b). No visible etching is observed up to 30 min and a small and asymmetrical pattern is observed at ~100 min. Unlike the experiments in absence of **B**, the corrosion pattern seems more symmetrical at 160 min and entirely symmetric at 300 min. This symmetrical corrosion pattern was also observed in the TSC (Supplementary Fig. 1c). One explanation for the symmetrical pattern in longer reaction times (as in Fig. 4a, 300 min) is the effect of solution rotation (Supplementary Video 1) due to the Lorentz force, which reduces the cell wall blocking effect.

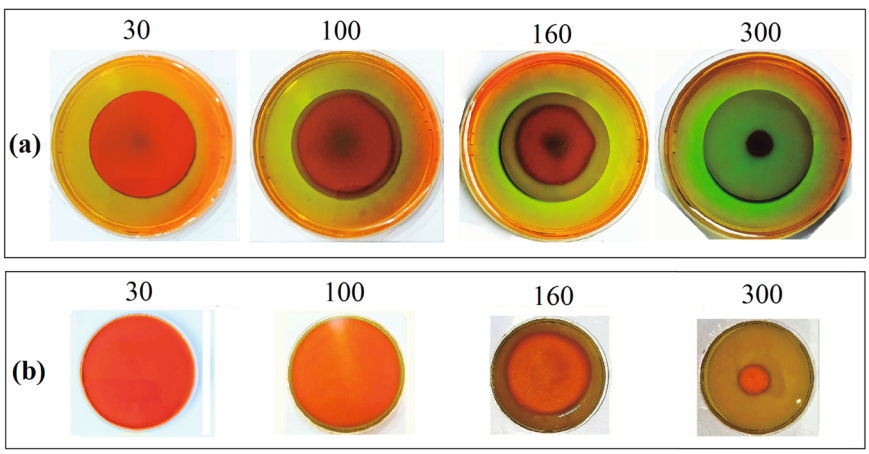


**Fig. 4 Corrosion of CCL disc in the presence of magnetic field using magnet bigger than CCL discs. a** Pictures of the corrosion process on the CCL disc in the SMBC setup (Fig. 8a-I). **b** Pictures of the corrosion process on the CCL disc in the BMSC setup (Fig. 8a-II).

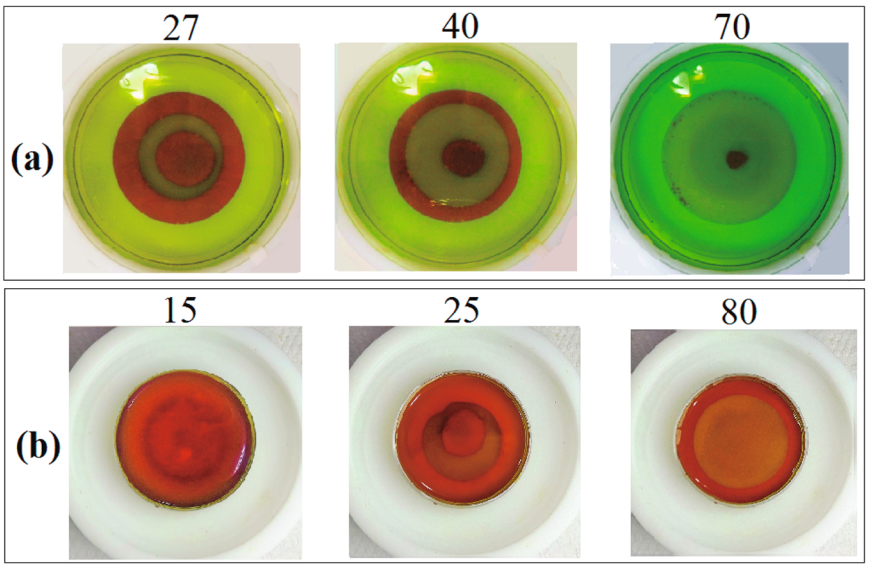


**Fig. 5 Corrosion of CCL disc using a magnet smaller than CCL disc. a** Pictures of the corrosion process on the CCL disc in the SMBC setup (Fig. 8b-III). **b** Pictures of the corrosion process on the CCL disc in the SMSC setup (Fig. 8b-IV).

### Corrosion using magnet smaller than CCL disc

Figure 5 shows pictures of the CCL disc in relation to reactions times in BC and SC etched in the $FeCl_3$ solution on the top of the smaller magnet (Fig. 8b). Supplementary Video 2 illustrates the MHD effect of **B** on the rotation of the corrosive medium in the SMBC setup. In these setups, the CCL discs are crossed by the strongest magnetic field gradient (MFG), called here inhomogeneous **B** (Fig. 8b) resulting in fast and peculiar corrosion processes.

Figure 5a shows pictures of the typical corrosion process on the CCL disc at 27, 40, and 70 min in the SMBC setup (Fig. 8b-III). Figure 5a shows that the CCL area on top of the magnet contour is rapidly etched, as it experiences the strongest MFG (Fig. 8b). The effect of MFG on corrosion of CCL disc is clear at 27 min (Fig. 5a). This result agrees with the Sagawa observation[4] using solid metal plate but is much easier to observe using in metallic thin film (CCL). At 40 and 70 min (Fig. 5a), the etching process increases in two directions, to the center and to the edge of the CCL disc. Figure 5a also shows that the copper film, at the center of the disc, remains up to 70 min even in this strong etching process. However, the copper film is hardly seen in the disc edge, indicating the protective effect of the homogeneous magnetic field.

Figure 5b also shows the strong effect of the MFG on the corrosion rate in the SMSC setup (Fig. 8b-IV). In this configuration, the effect of the MFG on the corrosion rate is clearly seen at ~15 min (Fig. 5b). At 25 min, corrosion is more pronounced than at 27 min (Fig. 5a) and it occurs toward the center of the disc and the magnet. This is better observed at 80 min, when the disc center is fully corroded. On the other hand, the disc edge is the last part corroded and corrosion is much slower in this area than in the SMBC setup (Fig. 5a). Therefore, the cell wall also exerts a strong effect on reducing the corrosion rate. Thus, when CCL is in the strong MFG (Fig. 8b), the etching process did not start at the disc edge, regardless of the size of the cells, as observed in the absence (Fig. 2) or in the presence of homogeneous **B** (Fig. 4). This was also observed in the TSC (Supplementary Fig. 1d). This strong corrosion effect observed in Fig. 5 is possibly due to the MFG, in the magnet contour that attracts preferentially the oxidant $Fe^{3+}$ that has the highest magnetic moment.

Supplementary Video 2 shows CCL corrosion using the **B** north pole of SM (Fig. 8b-III) in the first minutes of the etching process. The SMSC setup also shows a similar effect. This Supplementary Video shows a clockwise rotation on top of the magnet that is inverted when corrosion is performed using the **B** south pole also demonstrating the effect of the Lorentz force.

The rate of copper corrosion by $FeCl_3$ is a diffusion-controlled process that depends on both $Fe^{3+}$ and $Cu^{2+}$ transports[30,31]. The $Fe^{3+}$ moves from the solution to the metal surface and the $Cu^{2+}$ moves from the metal surface to the solution. Therefore, the metal at the edge of the disc is expected to be preferentially corroded (Fig. 2) because it is the region with rapid access to $Fe^{3+}$ from the solution on top of the disc as well as from the solution outside of the disc (Fig. 6a). It is also the region where $Cu^{+2}$ can diffuse from the metal surface to the solution on the disc top as well as from the solution outside of the disc.

The corrosion pattern observed in the presence of homogeneous **B** (Fig. 4) is similar to that observed in absence of **B** (Fig. 2). However, the corrosion rate is slower (Fig. 4) and the medium solution rotates (Supplementary Video 1). The solution rotates counterclockwise when the reactions are performed in the south magnetic pole (Supplementary Video 1) or clockwise in the north magnetic pole. These rotations indicate that positively charged particles are moving radially from the center of the disc to its border or negatively charged particles are moving in the opposite direction. The positive charges in the medium are the oxidant $Fe^{3+}$ and the reaction products $Fe^{2+}$ and $Cu^{2+}$ and the negative charge is the $Cl^-$. The $Fe^{3+}$ and $Cl^-$ are in high concentration and uniformly distributed in the solution and their diffusion in presence of **B** are not affected by the Lorentz force[32]. According to the diffusion model proposed in Fig. 6a, the $Cu^{2+}$ and $Fe^{2+}$ are the charged particles formed during the reaction that can move radially driven by the gradient concentration (light blue arrows).

Therefore, our hypothesis to explain the reduction of corrosion rate involves the rotation of these ions in the corrosive medium (Supplementary Video 1). This rotation is a typical magnetohydrodynamic effect since it correlates with fluid with charged particles subjected to the magnetic field. The complete understanding of the phenomenon is very complex because many parameters need to be taken into account: all charged particles, all magnetic particles, their masses and sizes, fluid viscosity, diffusions, external magnetic field intensity and geometry, physical barrier imposed by the Petri cell, CCL size, among others. These parameters obviously require a powerful simulation code in order to obtain more accurate predictions and understandings,

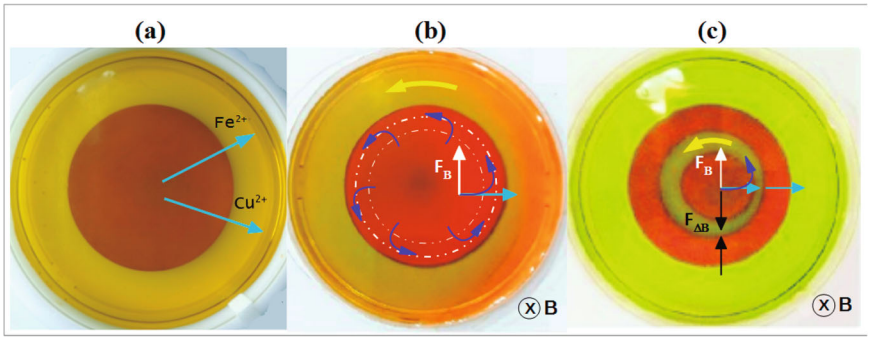


**Fig. 6 Schematic drawing of the effect of mass transport of iron and copper ions on the corrosion pattern and rate. a** Corrosion in absence of **B** showing the preferential movement of the cations. **b** Corrosion in presence of homogeneous **B** where the light blue arrow indicates the radial diffusion of $Cu^{2+}$ and $Fe^{2+}$, white arrow, the direction of $\mathbf{F_B}$ and dark blue curved arrows the deflection of the cations by $\mathbf{F_B}$, and the yellow arrow the rotation of corrosive medium, and **c** corrosion in presence of inhomogeneous **B** where the black arrows indicate the $F_{\Delta B}$.

which are not the scopes of this work. However, it is possible to have a phenomenological comprehension of the main actions driving the corrosion dynamics.

In the presence of homogeneous magnetic field **B** (Fig. 4), the $Cu^{+2}$ and $Fe^{2+}$ ions resulting from the reaction, preferentially leave the CCL disc due to the diffusion caused by the gradient concentration. Both appear at interface metal/solution and move to solution (Fig. 6b, light blue arrow).

Since **B** is perpendicular to the radial diffusion of the positive ions (Fig. 6b, light blue arrow), the effect of the magnetic part of the Lorentz force ($\mathbf{F_B}$), Eq. 1, must be considered[33].

$$\mathbf{F}_B = q\mathbf{v} \times \mathbf{B} \quad (1)$$

where q is the charge of the particle moving at velocity **v**.

The white arrow represents the magnetic part of the Lorentz force ($\mathbf{F_B}$), orthogonal to **v** and **B** and is a centripetal force that causes circular path for $Cu^{2+}$ and $Fe^{2+}$ (Fig. 6b, dark blue arrows) and consequently, the fluid rotation (Fig. 6b, yellow arrow) observed in Supplementary Video 1. Therefore, the deflection of the $Cu^{2+}$ and $Fe^{2+}$ from their radial trajectories causes a delay in the diffusion to outside of the metal surface, consequently decreasing the reaction rate.

On the other hand, when the CCL corrosion is performed in presence of inhomogeneous **B** an increase in corrosion rate is observed (Fig. 5). In the inhomogeneous **B** the MFG force ($\mathbf{F_{\Delta B}}$) must be considered[33] in addition to the action of the Lorentz force (observed in the rotation in the Supplementary Video 2). In presence of $\mathbf{F_{\Delta B}}$ (black arrows), the paramagnetic ions experience a force that is proportional to the strength of the MFG and to the magnetic momenta of the ions. Since $Fe^{+3}$ has the highest magnetic momentum among the ions in the medium, it is attracted to the strongest MFG force (Fig. 8b). Therefore, $\mathbf{F_{\Delta B}}$ increases the $Fe^{3+}$ concentration on the metal surface in the center of the CCL disc (Figs. 5 and 6c), increasing the corrosion rate. The effects of the magnetic field **B** described for BC (Fig. 6) can also be used to explain the pattern and the corrosion rate observed in SC experiments (Figs. 4b and 5b).

Figure 7 summarizes the main phenomena observed in the CCL discs, in BC and SC and in presence of inhomogeneous and homogeneous magnetic field. The corrosions in presence of inhomogeneous or homogeneous magnetic field were always, respectively, faster and slower than the corrosion in absence of **B**, independently of the cell size. The corrosion pattern at the end of depends on the cell size.

In conclusion, in this study, we demonstrated a simple and effective way to visually monitor and record the corrosion rate and its patterns *in operando* under several experimental conditions using CCL film. The CCL experiments showed an asymmetrical

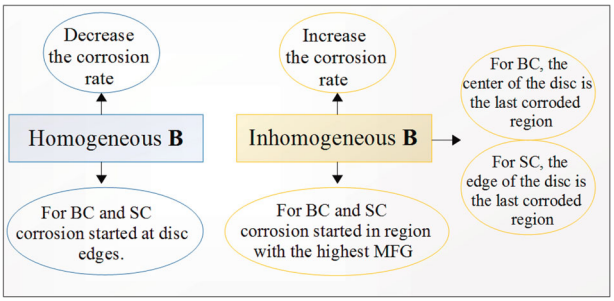


**Fig. 7 Schematic summary of the main phenomena observed in the CCL discs, in BC and SC and in presence of inhomogeneous and homogeneous magnetic field.** The corrosions in presence of inhomogeneous or homogenous magnetic field were always, respectively, faster and slower than the corrosion in absence of **B**, independently of the cell size. The corrosion pattern at the end of depends on the cell size.

corrosion pattern when the discs were not leveled or when the disc edges were blocked by the cell wall. The CCL experiments also showed a decrease or increase in the corrosion rate when the reactions were performed in the presence of homogeneous or inhomogeneous **B**, respectively. Corrosion in the presence of **B** shows clockwise or counterclockwise rotations, depending on the magnetic field orientation indicating the presence of the Lorentz force. The corrosion experiments proposed in this work could also be performed with other metallic thin films in inert substrate with several corrosive media. This procedure provides valuable information on the metal corrosion process in several environments, an important aspect for academic and industrial research.

## METHODS

We performed the corrosion experiments using single-sided CCL with a 0.1-mm copper layer deposited in 1.5-mm composite substrate and $FeCl_3$ solution, as the corrosive agent. The CCL was cut into circular disks with 51 mm in diameter and the copper surface was degreased, polished with 2500 mesh-coated abrasive, and dried prior to the corrosion experiments.

The CCL discs were concentrically placed on plastic Petri dishes, named SC and TSC that have the same internal diameter of 51.2 mm and a height of 9 and 25 mm, respectively and BC that has an internal diameter of 83.5 mm and a height of 13 mm. The corrosive medium comprised 30 ml of $FeCl_3$ solution, prepared by dissolving 100 g of $FeCl_3$ in 250 ml of distillated water. The SC could not hold the 30 ml solution thus TSC was initially used. However, the CCL disc was not visible in TSC due to the thicker layer of the corrosive medium (Supplementary Fig. 1a). Therefore, for real-time measurements, the experiments with SC were performed by adding three times volumes of 10 ml of $FeCl_3$ solution consecutively after each time that

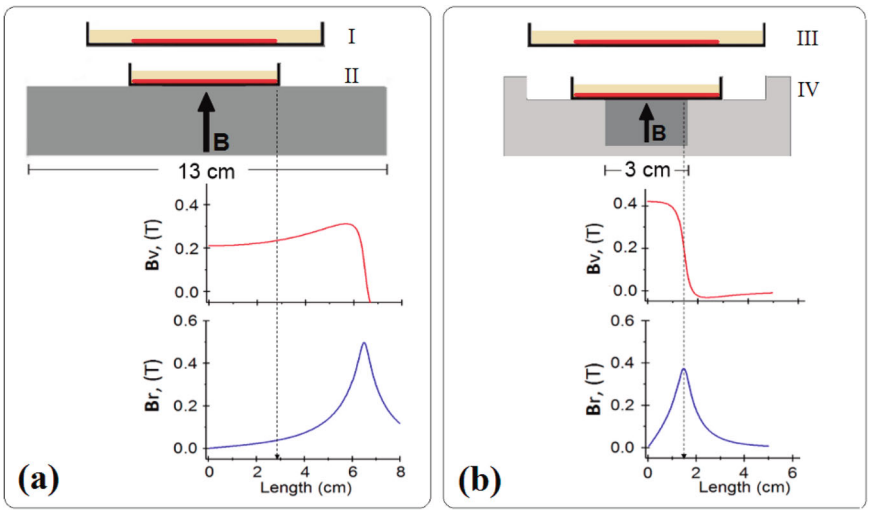


**Fig. 8 Experimental setups for corrosion in presence of magnetic field. a** Schematic drawing of the experimental setups for the BMBC (I) and BMSC (II). **b** for the SMBC (III) and SMSC (IV). The graphics show the calculated vertical (**B**v-red lines) and radial (**B**r-blue lines) components of the magnetic fields.

the corrosive medium changed from light yellow to green-brown opaque color (according to the corrosion rate). The corrosion reactions were carried out at 25 ± 2 °C and were monitored up to 300 min, using digital (cell phone or Gopro Hero 4) cameras[13,14,34–36]. The Gopro camera was preferentially used, as it has a plastic protective housing, an important feature to monitor the experiments in harsh corrosive environments.

The corrosion experiments were performed in the presence and absence of magnetic fields. The sources of magnetic fields were two cylindrical NdFeB permanent magnets named big magnet (BM) and small magnet (SM), with 130 mm in diameter and 25 mm in height and 30 mm diameter and 19 mm in height, respectively.

Figure 8a shows the diagram for the big magnet-big cell—BMBC (I) and big magnet-small cell—BMSC (II). Figure 8b displays the diagram for the small magnet-big cell—SMBC (III) and small magnet-small cell—SMSC (IV) setups. The magnets (dark gray), Petri cells (black), CCL discs (red), and $FeCl_3$ solutions (light yellow) are schematically represented in Fig. 8. The light gray part at Fig. 8b (top) is a Teflon piece that houses the small magnet and the cells. The graphics with red and blue lines are the calculated vertical (**B**v) and radial (**B**r) components of the magnetic fields, respectively. The dashed lines are used to guide the eyes and show that the CCL disc is in the homogenous region (Fig. 8a), which is crossed by the strongest magnetic field components and MFGs in Fig. 8b. The **B**v red lines and **B**r blue lines were calculated at 2 mm (copper surface) above the magnet surface, using FEMM (Finite Element Method Magnetics, an open-source code found at https://www.femm.info/wiki/HomePage).

## DATA AVAILABILITY

The authors declare that all data supporting the findings of this study are available within the paper and its Supplementary information files.

Received: 20 September 2021; Accepted: 23 February 2022;
Published online: 24 March 2022

## REFERENCES

1. Hansson, C. M. The impact of corrosion on society. *Metall. Mater. Trans. A.* **42**, 2952–2962 (2011).
2. Sastri, V. S. *Challenges in Corrosion: Costs, Causes, Consequences, and Control.* R. W. Revie (ed) Ch. 2 (John Wiley & Sons, 2015).
3. Koch, G. *Trends in Oil and Gas Corrosion Research and Technologies.* A. M. El-Sherik (ed) Ch. 1 (Woodhead Publishing, 2017).
4. Sagawa, M. Effect of a local magnetic-field on the dissolution of copper and iron in nitric-acid solution. *Trans. Jpn. Inst. Met.* **23**, 38–40 (1982).
5. Shinohara, K. & Aogaki, R. Magnetic field effect on copper corrosion in nitric acid. *Electrochemistry* **67**, 126–131 (1999).
6. Kountouras, D. T., Vogiatzis, C. A. & Touknidas, S. S. Preventing or accelerating galvanic corrosion through the application of a proper external magnetic field. *Corros. Eng. Sci. Technol.* **49**, 603–607 (2014).
7. Sueptitz, R., Tschulik, K. U. M., Gebert, A. & Schultz, L. Impact of magnetic field gradients on the free corrosion of iron. *Electrochim. Acta* **55**, 5200–5203 (2010).
8. Tang, Y. C., Gonzalez-Torreira, M., Yang, S. & Davenport, A. J. 2003. Effects of magnetic fields on corrosion. *J. Corros. Sci. Eng.* **6**, 46 (2003).
9. Ang, L. Y., Othman, N. K. & Jalar, A. The effect of magnetic field on copper in various corrosive medium. *AIP Conf. Proc.* **1614**, 26–29 (2014).
10. Lu, Z., Huang, D., Yang, W. & Congleton, J. Effects of an applied magnetic field on the dissolution and passivation of iron in sulphuric acid. *Corros. Sci.* **45**, 2233–2249 (2003).
11. Nasher, L. S. H. & Shalash, L. A. B. T. Study the effect of magnetic field on the corrosion of steel in sodium chloride solution (NaCl). *Misan J. Acad. Stud.* **9**, 30–38 (2010).
12. Ghabashy, M. E., Sedahmed, G. H. & Mansour, I. A. S. Effect of a magnetic field on the rate of diffusion-controlled corrosion of metals. *Br. Corros. J.* **17**, 36–37 (1982).
13. Sisso, O., Dor, S., Eliyahu, D., Sabatani, E. & Eliaz, N. Corrosion inhibition of copper in ferric chloride solutions with organic inhibitors. *npj Mater. Degrad.* **4**, 1–16 (2020).
14. Nammi, S., Sooraj, S., Amroop, B. S. & Vasa, N. hybrid laser scribing and chemical etching technique using pulsed $Nd^{3+}$:YAG laser to fabricate controlled micro channel profile. *J. Laser Micro Nanoeng.* **13**, 150–154 (2018).
15. Wang, B., Petrossians, A. & Weiland, J. Reduction of edge effect on disk electrodes by optimized current waveform. *Ieee. Trans. Biomed. Eng.* **61**, 2254–2263 (2014).
16. Simillion, H., Steen, N. V., Terryn, H. & Deconinck, J. Geometry influence on corrosion in dynamic thin film electrolytes. *Electrochim. Acta* **209**, 149–158 (2016).
17. Fytianos, G., Ucar, S., Grimstvedt, A., Svendsen, H. F. & Knuutila, H. Corrosion evaluation of MEA solutions by SEM-EDS, ICP-MS and XRD. *Energy Procedia* **86**, 197–204 (2016).
18. Schindelholz, E. J. et al. Electrochemical aspects of copper atmospheric corrosion in the presence of sodium chloride. *Electrochim. Acta* **276**, 194–206 (2018).
19. Grachev, A. V. et al. Measuring corrosion rate and protector effectiveness of advanced multilayer metallic materials by newly developed methods. *Heliyon* **4**, e00731 (2018).
20. Shrestha, B. R. et al. Real-time monitoring of aluminum crevice corrosion and its inhibition by vanadates with multiple beam interferometry in a surface forces apparatus. *J. Electrochem. Soc.* **162**, C327–C332 (2015).
21. Yuan, B. Y., Wang, C., Li, L. & Chen, S. H. Investigation of the effects of the magnetic field on the anodic dissolution of copper in NaCl solutions with holography. *Corros. Sci.* **58**, 69–78 (2012).
22. Weier, T. et al. Confinement of paramagnetic ions under magnetic field influence: Lorentz versus concentration gradient force based explanations. *Electrochem. Commun.* **9**, 2479–2483 (2007).
23. Monzon, L. M. A. & Coey, J. M. D. Magnetic fields in electrochemistry: the Lorentz force, a mini-review. *Electrochem. Commun.* **42**, 38–41 (2014).
24. Hu, J., Dong, C., Li, X. & Xiao, K. Effects of applied magnetic field on corrosion of beryllium copper in NaCl solution. *J. Mater. Sci. Technol.* **26**, 355–361 (2010).

25. Gomes, B. F., Lobo, C. M. S. & Colnago, L. A. Monitoring electrochemical reactions in-situ with low field NMR: a mini-review. *Appl. Sci.* **9**, 498–506 (2019).
26. Lobo, C. M. S. et al. Improving *in operando* low field NMR copper electrodeposition analyses using inductively coupled coils. *Electrochim. Acta* **298**, 844–851 (2019).
27. Benders, S., Gomes, B. F., Carmo, M., Colnago, L. A. & Blümich, B. In-situ MRI velocimetry of the magnetohydrodynamic effect in electrochemical cells. *J. Magn. Reson.* **312**, 106692 (2020).
28. Silva, P. F. et al. Electrochemical NMR spectroscopy: Electrode construction and magnetic sample stirring. *Microchem. J.* **146**, 658–663 (2019).
29. Blaha, F. Use of a magnetic field in detecting corrosion currents. *Nature* **166**, 607 (1950).
30. Habu, S. & Yoshihiro, Y. Studies of copper etching in ferric chloride solutions. *Ind. Eng. Chem. Process Des. Dev.* **27**, 511–514 (1982).
31. Salzberg, H. W., Knoetgen, H. & Molless, A. M. Rate of dissolution of silver in aqueous ceric sulfate solutions. *J. Electrochem. Soc.* **98**, 31–36 (1951).
32. Abdoli, I. & Sharma, A. Stochastic resetting of active Brownian particles with Lorentz force. *Soft Matter* **17**, 1307–1316 (2021).
33. Monzon, L. M. A. & Coey, J. M. D. Magnetic fields in electrochemistry: the Kelvin force. A mini-review. *Electrochem. Commun.* **42**, 42–45 (2014).
34. Moraes, E. P., Confessor, M. R. & Gasparotto, L. H. S. Integrating mobile phones into science teaching to help students develop a procedure to evaluate the corrosion rate of iron in simulated seawater. *J. Chem. Educ.* **92**, 1696–1699 (2015).
35. Igoe, D. & Parisi, A. V. Characterization of the corrosion of iron using a smartphone camera. *Instrum. Sci. Technol.* **44**, 139–147 (2016).
36. Vogel, G. Creeping corrosion of copper on printed circuit board assemblies. *Microelectron. Reliab.* 64, 650–655 (2016).

## ACKNOWLEDGEMENTS

This study was supported by CNPq that provided the scholarships under the process number 142238/2017-1 and 302866/2017-5, and by FAPESP grants numbers 2019/13656-8 and 2021/12694-3.

## AUTHOR CONTRIBUTIONS

C.I.N.M. designed and performed the experiments, analyzed and discussed the results, and wrote the paper; G.T. supervised the experiments, discussed the results, and reviewed the paper; L.A.C. conceived the project, provided the materials, designed and supervised the experiments, discussed the results, and reviewed and approved the paper.

## COMPETING INTERESTS

The authors declare no competing interests.

## ADDITIONAL INFORMATION

**Supplementary information** The online version contains supplementary material available at https://doi.org/10.1038/s41529-022-00233-5.

**Correspondence** and requests for materials should be addressed to Luiz Alberto Colnago.

**Reprints and permission information** is available at http://www.nature.com/reprints

**Publisher's note** Springer Nature remains neutral with regard to jurisdictional claims in published maps and institutional affiliations.